Study on dilution behavior of an oscillating jet in current environments using large eddy simulation

Wanru Zhang,[1] Zhenshan Xu,[1,2,a)] Shuqiao Fang,[3,4] Shunqi Pan,[5] Yongping Chen,[1,2]

AFFILIATIONS

[1]College of Harbor, Coastal and Offshore Engineering, Hohai University, Nanjing 210098, China

[2]The National Key Laboratory of Water Disaster Prevention, Hohai University, Nanjing 210098, China

[3]Key Laboratory of Nearshore Engineering Environment and Ecological Security of Zhejiang Province, Second Institute of Oceanography, Ministry of Natural Resources, Hangzhou 310012, China

[4]Key Laboratory of Ocean Space Resource Management Technology, Ministry of Natural Resources, Marine Academy of Zhejiang Province, Hangzhou 310012, China

[5]Hydro-environmental Research Centre, School of Engineering, Cardiff University, Cardiff, CF24 3AA, UK

[a)]**Author to whom correspondence should be addressed:** zsxu2006@hhu.edu.cn

ABSTRACT

The mixing behavior of an oscillating jet under the influence of currents remains incomprehensive. This study uses a three-dimensional large eddy simulation (LES) model to investigate the phase-averaged and time-averaged concentration distribution of three-dimensional scalar structures in the oscillating jet under a current environment. The effects of dimensionless parameters on dilution characteristics are also analyzed. The results indicate that increasing the jet-current velocity ratio (R_{jc}) and the amplitude-jet velocity ratio (R_{aj}), while decreasing the Strouhal number (S_t), can enhance the dilution capacity of the receiving water. To quantify the oscillatory effect of jets on the initial dilution of wastewater discharge, semi-empirical equations for the cross-sectional minimum dilution (S_c) and the visible diffusion area ($A_{25\%}$) of the oscillating jet in a current environment are developed using the least-squares method. The oscillatory nature of the jets is found to behave similarly to wave effects. Furthermore, the empirical equations for the initial

dilution of oscillating jets in current environments are structurally consistent with those for non-oscillating jets in wave-current coexisting environments. This study highlights the positive impact of oscillating jets on mixing and dilution.

I. INTRODUCTION

In recent years, global economic development and population growth have led to large volumes of domestic sewage and industrial wastewater being discharged into the sea. This influx has degraded near-shore seawater quality, exacerbated eutrophication, and posed significant threats to the reproduction and growth of marine organisms, thereby severely impacting the ecological structure of the oceans and the overall quality of the aquatic environment. Industrial wastewater, as well as discharges from thermal and nuclear power plants and desalination plants, are typically released into the sea with considerable momentum, often exhibiting buoyant jet behavior. The dilution and diffusion processes during jet discharge occur in two stages: initial dilution and subsequent diffusion. The initial dilution stage is particularly critical, as it substantially influences the subsequent dispersion of pollutant concentrations. Therefore, it is essential to study and analyze the dilution dynamics of jet streams in the near-field region. Enhancing the initial dilution of pollutants during jet discharge can reduce the extent of the wastewater mixing zone, contributing to water quality regulation and marine environmental protection.

Currently, the predominant method for discharging industrial wastewater and sewage involves the use of non-oscillatory jets with constant discharge rates. The characteristics of mean flow, turbulence, and entrainment significantly affect the trajectory and mixing behavior of jets.[1] Extensive research has been conducted on the mixing behavior of these non-oscillatory jets in current environments. The factors influencing the initial dilution of the jet can be broadly classified into two categories: jet parameters and background flow field parameters. Jet parameters include initial velocity, density, discharge aperture, geometry, and discharge angle, while background flow field parameters mainly refer to current velocity. Among these, the jet-current velocity ratio is the most critical factor influencing the dilution and motion patterns of non-oscillatory jets. Many studies have examined the effects of varying this ratio on the motion and diffusion of jets. For example, Moawad and Rajaratnam[2] measured the concentration field at different jet-current velocity ratios and developed an empirical equation for the minimum dilution. Muppidi and Mahesh[3] performed numerical simulations for jet-current velocity ratios of 1.5 and 7.5, and analyzed the trajectory of circular jets in a current. Megerian et al.[4] conducted experiments with jet-current velocity ratios ranging from 1 to 10, and revealed that significant differences in the shear layer of the current jet strongly depend on the jet-current velocity ratio.

In addition to altering the jet-current velocity ratio, many researchers have focused on investigating other factors that can enhance the initial dilution of jets from different perspectives, such as the discharge angle of the jet which can significantly affect its mixing and dilution behaviors.[5] Zeitoun et al.[6] examined discharge angles of 30°, 45°, 60°, and 90°, and found that the greatest dilution occurred at a 60° angle. Roberts et al.[7] analyzed the impact of discharge angle on jet dilution in a current environment, showed that jets with the maximum rise height result in a greater downstream dilution compared to the counter-flow direction. Kikkert et al.[8] conducted a numerical analysis of the trajectory and dilution characteristics of negatively buoyant jets with discharge angles from 0° to 75° and proposed a predictive formula closely matching experimental data. Roberts et al.[9, 10] investigated discharge angles of 0°, 45°, and 90°, and discovered that a 90° diffuser provided the best dilution in terms of centerline dilution, wastewater field thickness, and spreading width. The number, geometry, and aperture size of jet diffuser nozzles also affect the mixing behavior of the jet. Roberts and Snyder[11, 12] found that increasing the number of discharge nozzles decreased dilution, while Lai et al.[13] suggested that porous or rose-type diffusers could enhance initial jet dilution by adjusting the nozzle shape and discharge angle. Sharp[14] proposed using a buoyant wall jet to improve dilution via the Coanda effect after the jet exits the injector. Noutsopoulos and Yannopoulos[15] discovered that placing disc obstructions at various locations along the jet outlet, and proposed a functional relationship between the axial concentration outside the discs and the effectiveness of dilution when the discs are optimally positioned.

Wastewater discharge typically occurs in non-stationary receiving waters, making it essential to fully understand the impact of background flow fields on jet mixing processes due to the complex fluid interactions and diffusion patterns involved.[16, 17] Jet dilution is strongly influenced by wave motion. In the presence of waves, the jet region is generally divided into three sections: the curved section, the transition section, and the fully developed section.[18, 19] As wave intensity increases, the lateral distribution of jet velocity may exhibit three distinct patterns: Gaussian, flat-peak, and bimodal distributions. The oscillatory nature of waves alters the jet's trajectory and increases velocity fluctuations in the surrounding flow field. Key wave parameters, such as wave height, period, and phase, significantly affect jet motion and dilution characteristics in wave environments. Ryu et al.[20] used PIV techniques to measure the instantaneous velocity field of a horizontal circular pipe jet in a shallow water environment. They investigated how variations in wave amplitude and phase influenced the jet, finding that surface wave amplitude had a more significant impact on jet diffusion than wave phase. Yuan[21] developed a three-dimensional numerical model of a vertical turbulent jet in a shallow water environment to study the effects of various wave parameters on pollutant diffusion. His findings showed that jet dilution is primarily influenced by the ratio of wave amplitude to the jet's extended half-width along the water depth. Chang et al.[22] conducted experimental measurements of jet velocity fields under varying wave conditions in both deep and shallow waters. They found that jet entrainment is stronger in shallow waters and under steeper wave conditions, concluding that the most critical factor affecting jet entrainment strength is the momentum ratio between the wave and the jet.

The combined action of waves and currents enhances the mixing and dilution of jets with surrounding water. The wastewater discharge projects to the sea are often located in areas with strong oceanic dynamics, such as waves and tidal currents, to optimize dilution through vigorous mixing between buoyant jets and surrounding water.[23, 24] Chyan and Hwung[25] investigated the flow field of a vertical jet in a wave environment using flow visualization techniques, finding that pollutant concentration dilution increased significantly in the presence of waves. Hsiao et al.[26] studied the behavior of a turbulent round tube jet under the influence of regular waves using PIV, concluding that jet width, turbulence intensity, and Reynolds stress increased notably. More recently, Xu et al.[27-29] employed a large-eddy simulation model to conduct numerical simulations of three-dimensional jet motion in a wave environment. They explored jet dilution dynamics in detail and developed an empirical formula to describe jet dilution under wave action. Fang et al.[30] examined the physical mechanisms behind the vertical uplift of buoyant jets and established three semi-empirical equations. These equations quantified the influence of waves and buoyancy on the mixing behavior of buoyant effluent discharge in wave-current coexisting environments.

In recent years, research on the motion patterns and dilution effects of periodic oscillating jets in current environments has expanded, drawing parallels to the periodic oscillation of waves. Hsu and Huang[31] found that oscillating jets disperse more quickly and over a wider area than current-only environments, with lower Strouhal numbers leading to enhanced dilution and dispersion. Marcum et al.[32] demonstrated that the amplitude and frequency of oscillating jets significantly influence their kinematic patterns and diffusion characteristics through physical experiments. Arote et al.[33] reported numerical investigations for analyzing spatially oscillating planar jets by solving Navier–Stokes equations coupled with the volume of fluid method. However, most studies on oscillating jets have been limited to two-dimensional analyses, with fewer investigations into three-dimensional dilution behavior and the development of related empirical equations.

The main aim of this research is to investigate the three-dimensional mixing behaviors of a vertical round oscillating jet in a current environment using the method of large eddy simulation (LES) and establish relevant equations. The remaining part of this paper is organized as follows: Section 2 outlines the numerical model, boundary conditions, model validation, dimensional analysis, and applications. Section 3 includes the results and discussion on phase-averaged and mean scalar structure, the effect of dimensionless parameters, and the comparison of dilution characteristics between the oscillating jets in the current environment and jets in the wave-current coexisting environment. Finally, conclusions are provided in Section 4.

II. METHODOLOGY

A. Numerical model

The large eddy simulation (LES) model, which utilizes spatially filtered Navier-Stokes equations, is employed in this study. To address the free surface tracking problem, the model uses σ-coordinates in the vertical direction. The numerical method applies the operator splitting technique,[34] dividing the solution into three distinct steps: convection, diffusion, and pressure propagation. The convective term is discretized using the quadratic backward eigenline method combined with Lax-Wendroff averaging, while the diffusion term is handled via time-advanced, spatial-centered difference discretization. Poisson's equation is then solved using the conjugate gradient algorithm. A comprehensive study of the jet flow structure in a wave-current coexisting environment has been conducted using this model, with further details provided in Xu et al. [27-29]

B. Boundary conditions

The current outlet boundaries utilize the modified artificial sponge layer method with zero gradient conditions. Lateral boundaries are defined with impermeable boundary conditions, where the wall-normal component of each physical quantity is zero. The bottom boundary applies the wall function method for pressure and the slip condition for velocity.

The exit turbulence of the oscillating jet is generated using the Synthetic Eddy Method (SEM) to meet the stochastic requirements of turbulent velocity components.[35] The SEM is based on several key assumptions: turbulence consists of a set of sequential structures generated at the inlet boundaries; the spatiotemporal characteristics of these structures are defined by a shape function; and turbulence can be modeled using stochastic eddies with specific positions and orientations. The SEM method is described as follows.

Take the simpler one-dimensional turbulence boundary as an example, as shown in FIG. 1. To generate a unidirectional velocity signal in the interval [a, b], it is necessary to construct a vortex motion plane $\Delta x \times \Delta y$. Each vortex has two attributes: coordinates (x_i, y_i) and length scale σ_i. The vortex center position in the figure is denoted by '*'. For simplicity, each vortex scale is temporarily defined as being equal to σ. The synthetic vortices are randomly distributed on the vortex plane, ensuring that every point on the turbulence boundary has a chance to be surrounded by vortices.

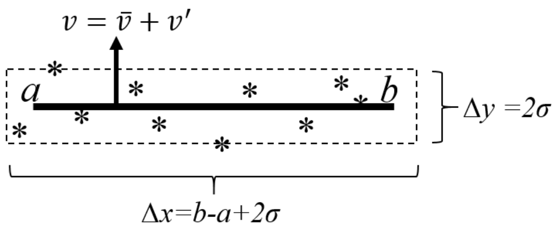

FIG. 1. Vortex plane of motion.

Taking the simple one-dimensional turbulence boundary as an example, as shown in FIG. 1, to generate a unidirectional velocity signal in the interval [a, b], it is necessary to construct a vortex motion plane $\Delta x \times \Delta y$. Each vortex has two attributes: location (x_i, y_i) and length (σ_i). The vortex center position in FIG. 1 is denoted by '*'. For simplicity, each vortex length scale is temporarily defined as being equal to σ. The synthetic vortices are randomly distributed on the vortex plane, ensuring that every point on the turbulence boundary has a chance to be surrounded by vortices.

Then, a shape function of the vortex (f_σ), which is tightly supported in the interval [a-σ: b+σ, -σ: σ] and satisfies the normalization condition is defined, as shown in Eq. (1). Each eddy is given a random variable characterizing the direction of the disturbance ε_i, which is chosen randomly only between +1 and -1 to ensure that the expectation of the velocity field pulsation is 0. Therefore, the velocity contribution of a particular eddy (with coordinate x_i and i denoting the number of the eddy) to a point (with coordinate x) on the turbulence boundary is expressed by Eq. (2), where $f_\sigma(x\text{-}x_i)\, f_\sigma(y_i)$ denotes the distribution of the velocity of the ith eddy at that point. Similarly, the velocity of the superposition of N eddies at a point (with coordinates x) on the turbulent boundary can be derived by Eq. (3).

$$\frac{1}{\Delta x \Delta y}\int_{\frac{-\Delta x}{2}}^{\frac{\Delta x}{2}}\int_{\frac{-\Delta y}{2}}^{\frac{\Delta y}{2}} f_\sigma(x) f_\sigma(y)\,dy\,dx = 1 \tag{1}$$

$$v'^{(i)}(x) = \varepsilon_i f_\sigma(x_i - x) f_\sigma(y_i) \tag{2}$$

$$v'(x) = \frac{1}{\sqrt{N}}\sum_{i=1}^{N} \varepsilon_i f_\sigma(x_i - x) f_\sigma(y_i) \tag{3}$$

The number of eddies in the computational domain is determined by $(b - a) / \sigma$ to ensure that the turbulence boundary is fully covered by eddies. The autocorrelation function at any two points on the turbulent boundary can be calculated using Eq. (4).

$$R_{vv}(r) = \frac{1}{\Delta x}\int_{-\Delta x/2}^{\Delta x/2} f_\sigma(x) f_\sigma(x + r)\,dx \tag{4}$$

The one-dimensional turbulence boundary $[a, b]$ is expanded to a two-dimensional planar turbulence boundary $[0, 0{:}\ L_y, 0{:}\ L_z]$ (shown as a blue area in FIG. 2), assuming that there is a mean flow velocity along the x-direction only. It is first necessary to construct a space for the motion of eddies in three-dimensional space, referred to as the vortex box, which has a volume of $[-\sigma_x, \sigma_x]\times[-\sigma_y, L_y + \sigma_x]\times[-\sigma_x, L_z + \sigma_x]$ to ensure that every point on the turbulence boundary can be surrounded by eddies. Similarly, the shape function of the eddies is tightly supported within the vortex box and satisfies the normalization condition. The vortices are randomly distributed throughout the vortex box and convect at a constant characteristic velocity. Assume that the coordinate of the i_{th} vortex at moment t is (x_i, y_i, z_i), and that the horizontal coordinate of this vortex changes to $x_i(t + dt) = x_i(t) + \overline{u}(y_i, z_i)\, dt$ moment $t + dt$. When a vortex moves out of the vortex box, it will randomly generate a vortex with the same length scale at an arbitrary position on the inlet boundary of the vortex box.

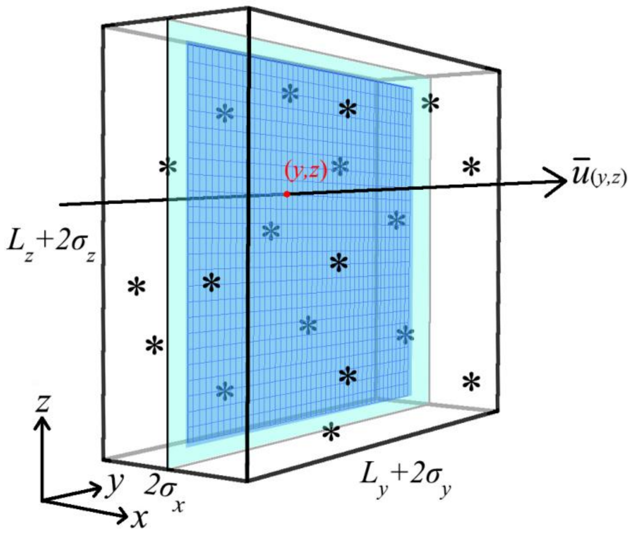

FIG. 2. Schematic diagram of a vortex box.

The velocities resulting from the superposition of N vortices at a specific point on the turbulent plane (0, y, z) at time t can be expressed as follows,

$$u_i(\underline{x},t) = \overline{u_i}(\underline{x}) + a_{ij}u'_j(\underline{x},t) \qquad (i,j=1,2,3) \tag{5}$$

$$u'_j(\underline{x},t) = \frac{\delta}{\sqrt{N}}\sum_{k=1}^{N}\varepsilon_j^k f_\sigma\left(\underline{x}-\underline{x}^k(t)\right) \qquad (j=1,2,3) \tag{6}$$

$$f_\sigma\left(\underline{x}-\underline{x}^k(t)\right) = \sqrt{\frac{V_B}{\sigma_x\sigma_y\sigma_z}}\, f\left(\frac{x-x^k(t)}{\sigma_x}\right) f\left(\frac{y-y^k}{\sigma_y}\right) f\left(\frac{z-z^k}{\sigma_z}\right) \tag{7}$$

$$f(\zeta) = \begin{cases} \sqrt{1.5}\left(1-|\zeta|\right) & |\zeta| \le 1 \\ 0 & |\zeta| > 1 \end{cases} \tag{8}$$

$$a_{ij} = \begin{pmatrix} \sqrt{R_{11}} & 0 & 0 \\ R_{21}/a_{11} & \sqrt{R_{22}-a_{21}^2} & 0 \\ R_{31}/a_{11} & \left(R_{32}-a_{21}a_{31}\right)/a_{22} & \sqrt{R_{33}-a_{31}^2-a_{32}^2} \end{pmatrix} \tag{9}$$

$$N \approx L_y \cdot L_z / \sigma_y \cdot \sigma_z \tag{10}$$

$$dt \approx 0.1\sigma_i / \overline{u}_i \tag{11}$$

where u_i, $\overline{u_i}$ and u_i' is the instantaneous, time average and turbulent flow velocities in the i-direction, respectively; a_{ij} is the Cholesky decomposition of the Reynolds stress tensor; δ is the turbulence amplification factor, set by default at 1.0; N is the number of vortices; ε_j^k is a random variable that characterizes the direction of the perturbation, which is randomly chosen between +1 and -1; V_B is the volume of the vortex box; $f(\zeta)$ is the shape function, which, according to Lu and

Dai,[36] is selected as the trigonometric function; dt is the time step.

In this study, the jet outlet is round with a diameter of 1.0 cm. However, for the numerical simulation of the jet outlet fitting process, a rectangular outlet is employed. To approximate the actual situation, this geometry is simplified to a square with an equivalent cross-sectional area, resulting in a side length of 0.886 cm. The mean flow velocity at the outlet boundary is characterized by velocities of 0 m/s in the y and z directions and 0.5 m/s in the x direction. The outlet is discretized into 1010 grids, and the simulation includes 25 vortices, each with a characteristic length of 0.004 m. The time step dt is set to 0.001 s. The Reynolds number for this configuration is calculated to be 4393, indicating that the flow mode is turbulent. During the simulation experiments, the turbulence amplification factor was set to 1.5, and the boundary condition on the jet outlet was established at 0.96.

C. Model validation

Experiments designed to validate the numerical model were conducted using a 46.0-m-long, 0.5-m-wide, and 1.0-m-deep wave flume with a water depth of 0.5 m. The specialized oscillating jet generator adjusts the current based on input signals to control the pump. Different groups of oscillating jet period T were 1.0 s, 1.5 s and 2.0 s, with an amplitude w_A=0.25 m/s. Flow velocity measurements used a Vectrino Profiler. The mean velocity of the jet (w_o) was 0.535 m/s, and the vertical flow velocity in the z/d section was measured in this experiment. The computational domain of the mathematical model is 9.0 m long, 0.5 m wide, and 0.5 m deep. The oscillating jet was positioned 4.0 m from the inlet boundary, with the jet pipe having a diameter of 1.0 cm. Numerical simulations were performed with identical parameter settings for all groups. The turbulence amplification coefficient was set to 3.0, the mean jet velocity to 0.535 m/s, and the Smagorinsky constant to 0.175. FIG. 3 to FIG.6 show the comparison between numerical results and experimental data in the jet in still water environment, oscillating jet in still water environment and current-only environment. The good agreement between the numerical and experimental results demonstrates the general accuracy of the LES model. Additionally, the validity of this approach has been confirmed in the LES simulation of a buoyant jet in stagnant water,[37] as well as a vertical round jet in the wave-current coexisting environment.[28] The validation results prove that the model can reasonably predict the distribution of vertical flow velocity along the water depth at different sections of the jet.

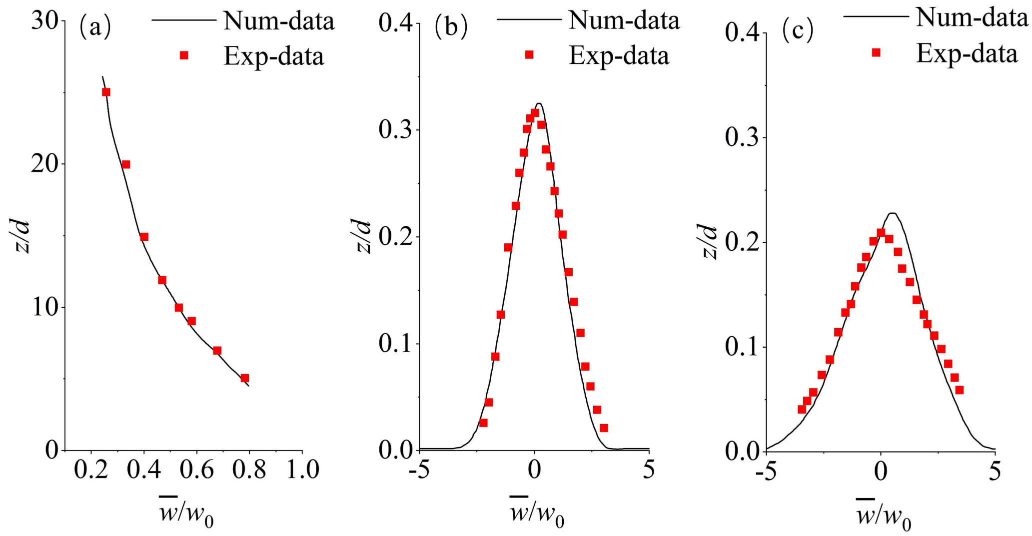

FIG.3. Comparison between numerical model results and experimental data of non-oscillating jet in still water environment: (a) Vertical velocity decay; (b) Velocity distribution on section *z*/*d*=15; (c) Velocity distribution on section *z*/*d*=25.

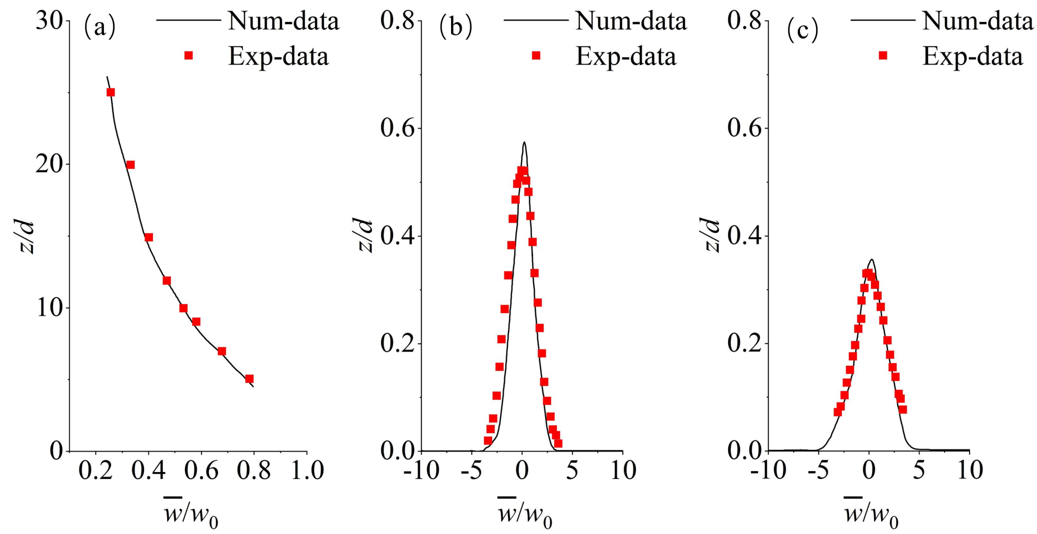

FIG.4. Comparison between numerical model results and experimental data of oscillating jet in the still water environment: (a) Vertical velocity decay, (b) Velocity distribution on section *z*/*d*=15, (c) Velocity distribution on section *z*/*d*=25.

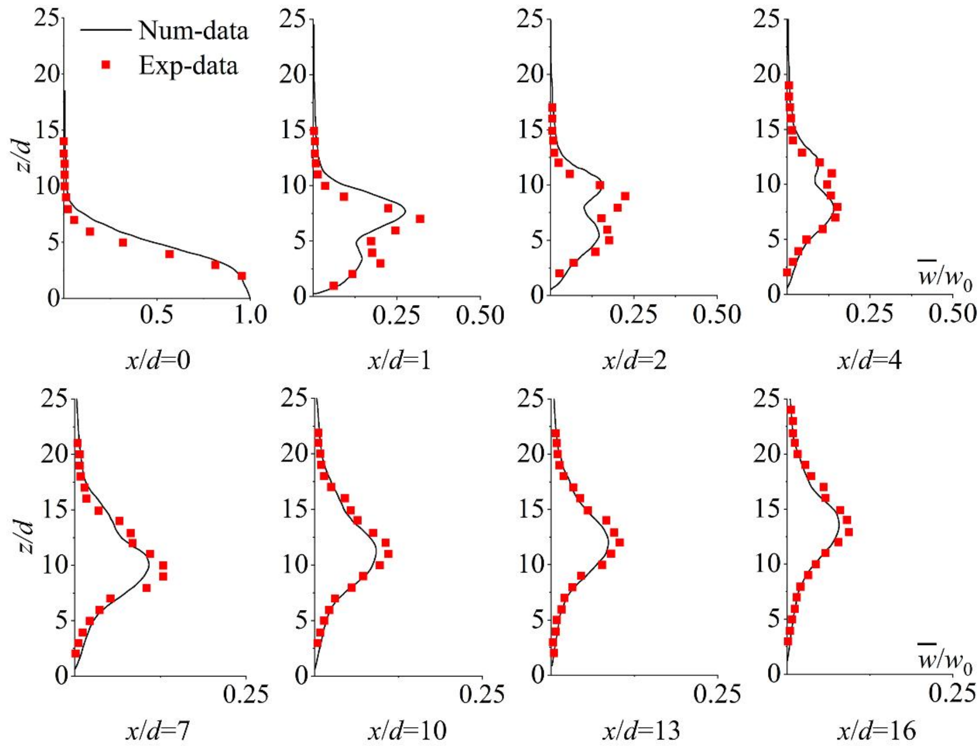

FIG.5. Comparison of mean vertical profiles on the vertical symmetrical plane (y/d=0) between numerical results and experimental data at eight downstream locations (x/d=0, 1, 2, 4, 7, 10, 13, 16) for the jet in the current-only environment.

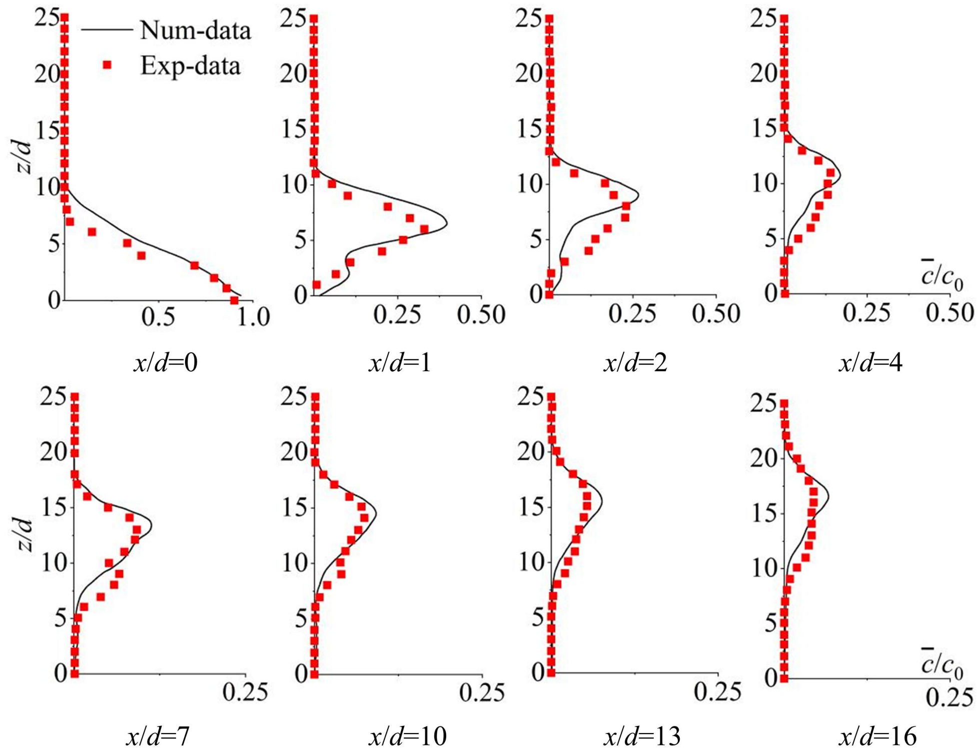

FIG.6. Comparison of mean concentration distribution on the vertical symmetrical plane (y/d=0) between numerical results and experimental data at eight downstream locations (x/d=0, 1, 2, 4, 7, 10, 13, 16) for the jet in the current-only environment.

D. Dimensional analysis

The motion of an oscillating jet in a current environment is influenced by two distinct factors. The first factor is the intrinsic properties of the jet, including the pipe diameter (d), mean velocity (w_0), oscillation period (T), and amplitude (w_A). The second factor is the background flow field parameters, specifically the current velocity (u_0). The above parameters are the most basic factors affecting jet motion characteristics. By combining these parameters, dimensionless parameters can be derived to describe the jet's motion characteristics. The jet-current velocity ratio (R_{jc}) is a key parameter for describing jet motion and mixing characteristics. The amplitude-jet velocity ratio (R_{aj}) reflects the influence of oscillation amplitude, and the Strouhal number (S_t) reflects the influence of the oscillation period. The formulas for these three dimensionless parameters are as follows:

$$R_{jc} = w_0 / u_0 \tag{11}$$

$$R_{aj} = w_A / w_0 \tag{12}$$

$$S_t = d / (u_0 / T) \tag{13}$$

According to the recommendation of Lee and Chu,[38] utilizing a combination of characteristic parameters, such as characteristic length, initial flow rate, and momentum can effectively analyze the cross-sectional dilution law and produce reliable fitting results. While the ambient fluid velocity can influence the magnitude of the levy length and momentum when waves are neglected, the impact of oscillating must be considered. Specifically, the amplitude of the oscillating jets should be incorporated into the characteristic velocity (w_{ch}), which is defined as follows:

$$w_{ch} = w_0 (1 + \alpha_{wc} \frac{w_A}{w_0}) \tag{14}$$

where α_{wc} is expressed as the parameter of the oscillatory action and the influence of the current on the jet, which can be calculated by the following equation:

$$\alpha_{wc} = \frac{4}{T} \int_0^{T/4} \cos \omega t dt \tag{15}$$

where ω is the oscillation frequency of the jet (ω = 2π/T). By integrating the calculation, we can obtain α_{wc} as 0.637, which characterizes the degree of contribution of the oscillation velocity to the characteristic velocity. The characteristic momentum M_{ch} of the oscillating jet is:

$$M_{ch} = 0.25\pi d^2 w_{ch}^2 \tag{16}$$

The physical meaning of the characteristic length scale L_m of an oscillating jet in a current environment is the relative strength of the oscillating jet to the current, which can be expressed by the following equation,

$$L_m = M_{ch}^{1/2} / u_0 \tag{17}$$

The combination of the above parameters can accurately reflect the jet dilution behavior. The dilution process can then be quantitatively described through curve fitting. Therefore, in this study, a sampling combination of characteristic parameters is employed to fit the concentration characteristic curve, ultimately leading to the derivation of an empirical formula for the concentration characteristics of oscillating jets in current environments.

E. Numerical cases

To fully describe the three-dimensional dilution characteristics of oscillating jets in a current environment and investigate the influence of each oscillation parameter on jet concentration, and derive empirical equations for initial dilution, in total 19 numerical experiments are conducted in this study. Amongst, one case is with current-only environment (DJ00) and 18 cases are with varying oscillation parameters. The model parameters of each case are presented in TABLE I, where the current velocities of cases CJ06 to CJ12 are 0.5 m/s as the R_{jc} comparison cases

TABLE I. Details of calculation cases and parameters of oscillating jet in a current environment.

Case	Jet mean velocity w_0 (m/s)	Current velocity u_0 (m/s)	Jet amplitude w_A (m/s)	Oscillation period T (s)	Amplitude-to-jet velocity ratio (R_{aj})	Strouhal number (S_t)
DJ00	0.40	0. 05	/	/	/	/
DJ01	0.40	0. 05	0.04	1.0	0.1	0.2
DJ02	0.40	0. 05	0.08	1.0	0.2	0.2
DJ03	0.40	0. 05	0.16	1.0	0.4	0.2
DJ04	0.40	0. 05	0.32	1.0	0.8	0.2
DJ05	0.40	0.05	0.04	2.0	0.1	0.1
DJ06	0.40	0. 05	0.08	2.0	0.2	0.1
DJ07	0.40	0. 05	0.16	2.0	0.4	0.1
DJ08	0.40	0. 05	0.32	2.0	0.8	0.1
DJ09	0.40	0. 05	0.04	4.0	0.1	0.05
DJ10	0.40	0. 05	0.08	4.0	0.2	0.05
DJ11	0.40	0. 05	0.16	4.0	0.4	0.05
DJ12	0.40	0. 05	0.32	4.0	0.8	0.05

CJ06	0.50	0. 05	0.1	2.0	0.2	0.1
CJ07	0.50	0. 05	0.2	2.0	0.4	0.1
CJ08	0.50	0. 05	0.4	2.0	0.8	0.1
CJ09	0.50	0. 05	0.05	4.0	0.1	0.05
CJ10	0.50	0. 05	0.1	4.0	0.2	0.05
CJ11	0.50	0. 05	0.2	4.0	0.4	0.05
CJ12	0.50	0. 05	0.4	4.0	0.8	0.05

III. RESULTS AND DISCUSSION

A. Phase-averaged scalar structure in the symmetrical plane

FIG.7 presents the phase-averaged velocity and concentration fields of the jet in the symmetric longitudinal section (y/d = 0) at four characteristic phases of Case DJ06. The oscillating jets, influenced by the current, display a distinct "effluent cloud", which is similar to the behavior observed in jets in a wave-current coexisting environment.[28] The sequence A1-B1-C1-D1-A2 can be interpreted as the formation and development of the effluent clouds throughout one oscillation cycle. At the 1/4 T, the impact height is at its lowest, while the curvature is at its maximum. During this phase, the jet column tilts upward, and the pollutant cloud gradually expands. As the jet velocity decreases around 1/2 T, the effluent cloud continues to develop and expand. By the 3/4 T, the jet column inclines downward, and the effluent cloud is carried downstream. Due to the interaction between the shear layer vortex and the current, convoluted suction occurs, causing the leading side of the shear layer vortex to expand and become incoherent. At this point, the impact height reaches its maximum and the curvature is at its minimum. The jet column experiences significant deflection due to the current. As the cycle reaches the T, the jet velocity increases, causing the jet column to tilt upward once again. This cyclical process aligns with the findings of Shi,[35] confirming that oscillating jets cause the effluent cloud to propagate downstream periodically. Hsu[31] identified different flow modes throughout this process: the jet-dominated mode at 1/4T, the transition mode at 1/2 T, the downwash mode at 3/4 T, and the current-dominated mode at T. The effluent clouds appear in every oscillation cycle, and the bending of streamlines indicates the locations of these clouds.

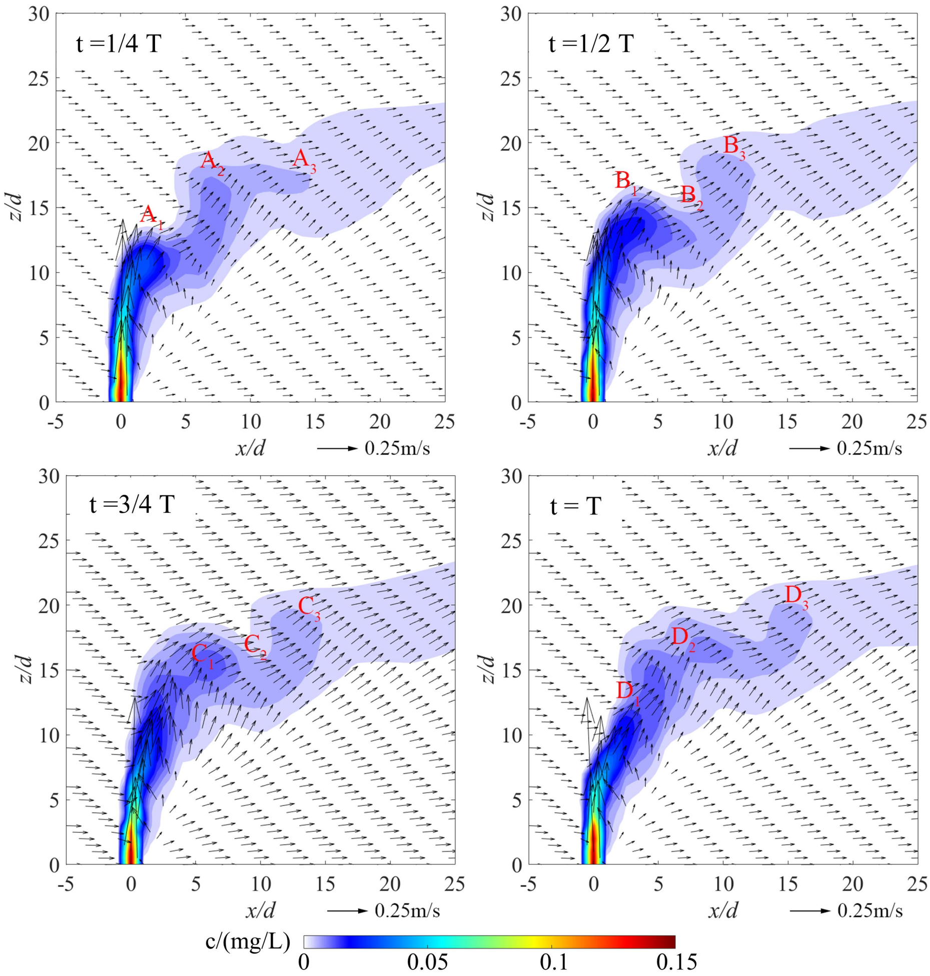

FIG.7. Phase-averaged flow structures and concentration distributionsat y/d=0 section under four typical phases of Case DJ06.

B. Time-averaged concentration field

FIG.8 illustrates the distributions of the time-averaged mass concentration of the jet at different downstream sections for 7 cases. It clearly shows that the presence of oscillating jets significantly increases the vertical width of the jets compared to the jet in current-only environment. The cross-sectional envelope shape of the jet in a current-only environment gradually transforms from a clustered oblate shape to a dispersed bipetal shape, becoming taller and narrower as it propagates downstream. In contrast, the oscillating jet behaves differently; as it moves downstream, its cross-section transitions from initially wide and elongated stripes to a more aggregated oblate shape. Due to the existence of the counter-rotating vortex pair (CVP) structure, the mean mass concentration in the downstream section of jets in a current-only environment exhibits two extreme values. In oscillating jets, the periodic oscillation alters the distribution of the mean mass concentration in the downstream section. Depending on the oscillation intensity, there may be two maxima in the downstream section due to the CVP structure (Case DJ04) or one maximum associated with the "effluent cloud" (Case DJ06). In Case DJ04, the maximum mean mass concentrations in the downstream section are found at the vortex center of the lower CVP structure. However, in Case DJ06, the maximum concentrations occur at the "effluent cloud" location. As the jet propagates downstream in Case DJ06, the initial single maximum mass concentration from the "effluent cloud" gradually evolves into two maxima, suggesting the possible development of a new CVP structure at the location of the "effluent cloud".

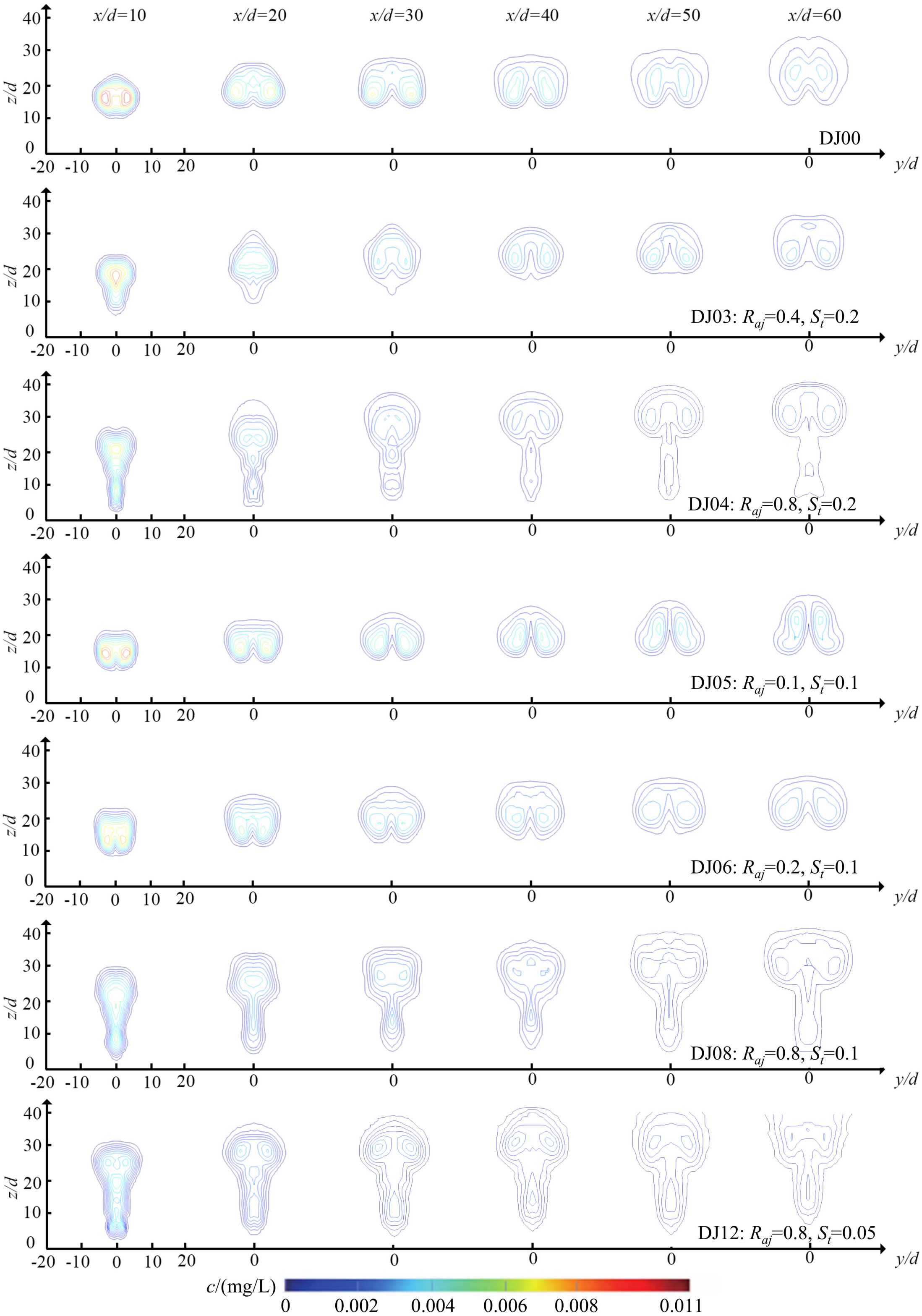

FIG. 8. Time-averaged concentration distributions on downstream sections

C. Effects of R_{jc}, R_{aj} and S_t on the concentration characteristics of oscillating jets

Lee and Chu[38] proposed that several key parameters be used to characterize the concentration at the cross-section downstream of a jet in a current-only environment: the mean maximum scalar concentration in the transverse planes (C_m) (or the cross-sectional minimum dilution (S_c=c_0/c_m)), vertical position of the concentration maximum (Z_s), width (R_h) and height (R_v) of the concentration contour of C = 0.25C_m (Fig. 9(a)). In this study, similar metrics are adopted to describe the concentration distribution in the downstream section of an oscillating jet in a current environment and the area of the concentration contour of 0.25 C_m is used to represent R_h and R_v (hereafter referred to as the jet visual area $A_{25\%}$) as shown in FIG. 9.

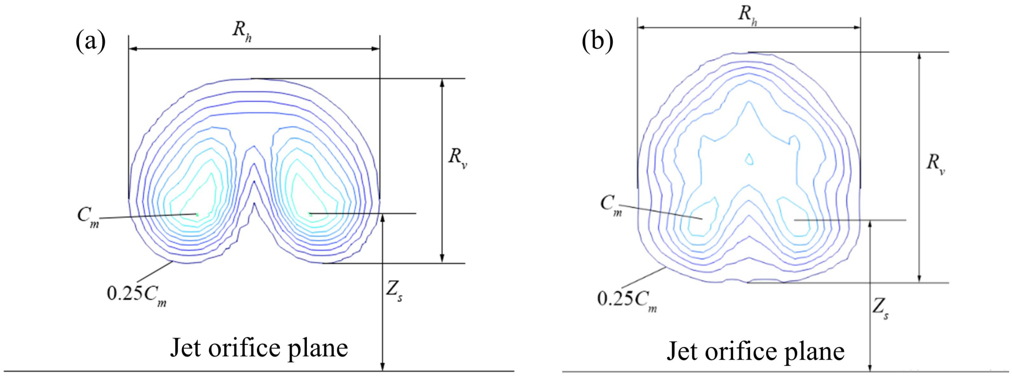

FIG. 9. Definition diagram of characteristic dilution parameters: (a) jet in the current-only environment, (b) oscillating jet in the current environment.

FIG. 10 illustrates the influence of three combined characteristic parameter (R_{jc}, R_{aj} and S_t) on the minimum dilution (S_c) along the downstream distance x/d. All three parameters impact Sc to varying degrees. As shown in FIG. 10(a), within the range of x/d from 0 to 40, the Case CJ08 exhibits a higher cross-sectional minimum dilution. However, when x/d exceeds 40, the minimum dilution for the Case DJ08 surpasses that of Case CJ08, despite the latter having a higher jet velocity. This due to higher jet velocity impacts the free surface of the receiving water earlier, completing dilution and ceasing further spreading. Additionally, as shown in FIG.10(b) and 10(c), S_c increases significantly with an increase in R_{aj} and a decrease in S_t. However, the S_c distribution curves of the two cases (DJ06 and DJ10) become nearly indistinguishable as S_t continues to decrease.

FIG. 11 exhibits the influence of three combined characteristic parameters (R_{jc}, R_{aj} and S_t) on the jet visual area $A_{25\%}/d^2$ along the downstream distance x/d. As R_{jc} and R_{aj} increase, the jet visual area ($A_{25\%}$) also increases [FIG. 11(a) and 10(b)]. In the range of x/d = 20-40, the $A_{25\%}$ of the Case CJ08 with larger R_{jc} is significantly higher than that of the Case DJ08, indicating that the effect of the R_{jc} on $A_{25\%}$ is very significant. FIG. 11(c) shows the effect of S_t, the distribution curve of cases

DJ10 and DJ06 are extremely close, while Case DJ02 is significantly lower than the other two cases.

FIG. 12 exhibits the influence of three combined characteristic parameters (R_{jc}, R_{aj} and S_t) on the Z_s along the downstream distance x/d. The Case CJ08, which has a larger R_{jc}, the Z_s are higher from the bottom bed, particularly when x/d exceeded 20. The disparity in Z_s distribution between the two cases also becomes more pronounced. When R_{aj} is large (cases DJ11 and DJ12), Z_s increases with a higher R_{aj}. However, when R_{aj} is smaller, there is no significant effect on the Z_s distribution. Regarding S_t, variations in S_t have minimal impact on the distribution of Z_s. Overall, the distribution of the vertical location of the minimum dilution (Z_s) is irregular. This irregularity arises from Z_s potentially occurring either at the vortex center of the CVP structure in the lower part of the jet or at the location of the "effluent cloud" in the upper part of the jet, depending on the amplitude of the jet oscillations.

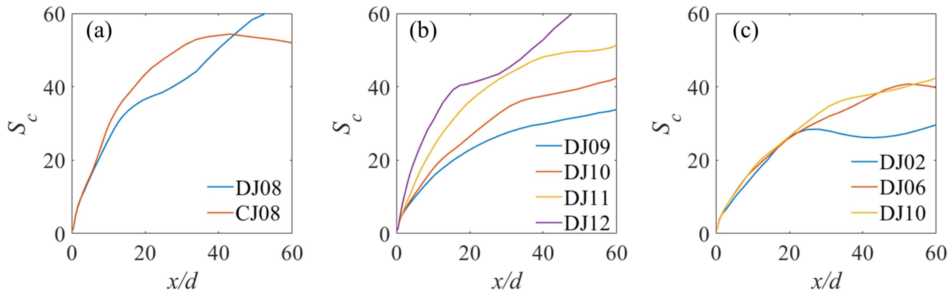

FIG. 10. Influence of parameters on the minimum dilution S_c along the downstream distance x/d, (a) R_{jc} comparison cases, (b)R_{aj} comparison cases, (c) S_t comparison cases.

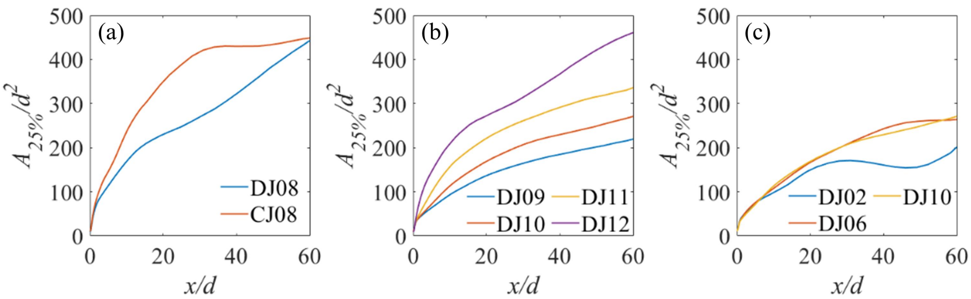

FIG. 11. Influence of parameters on the visible diffusion area $A_{25\%}/d^2$ along the downstream distance x/d, (a) R_{jc} comparison cases, (b)R_{aj} comparison cases, (c) S_t comparison cases.

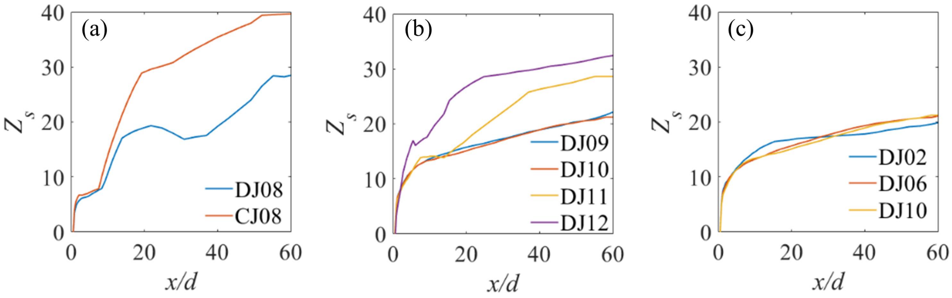

FIG. 12. Influence of parameters on the vertical location of minimum dilution Z_s along the downstream distance x/d, (a) R_{jc} comparison cases, (b)R_{aj} comparison cases, (c) S_t comparison cases.

D. Equation for vertical location of cross-sectional characteristic parameters

The jet-current velocity ratio (R_{jc}), amplitude-jet velocity ratio (R_{aj}), and Strouhal number (S_t) all influence the motion and mixing characteristics of the jets to varying degrees, and these parameters provide valuable insights into the dilution behavior of jets. However, due to the irregular distribution of vertical location of the minimum dilution (Z_s), this index is not fitted in the present study. Similar to the empirical formulas for non-oscillatory jets in a wave-current coexisting environment,[29] the characteristic velocity, momentum, length, and Strouhal number of jets for each case were calculated (TABLE II). With these characteristic parameters, the concentration parameter S_c and $A_{25\%}$ against the downstream distance x were made dimensionless, and the relevant indexes were fitted using the least-squares method. These results have significant practical implications for applications such as environmental assessment and oceanic drainage engineering design.

TABLE II. Characteristic parameters of oscillating jet in current environment.

case	w_{ch}	M_{ch} (*10^{-5})	L_m	S_t
DJ01	0.4255	1.4218	0.0754	0.2
DJ02	0.4510	1.5972	0.0799	0.2
DJ03	0.5019	1.9786	0.0890	0.2
DJ04	0.6038	2.8637	0.1070	0.2
DJ05	0.4255	1.4218	0.0754	0.1
DJ06	0.4510	1.5972	0.0799	0.1
DJ07	0.5019	1.9786	0.0890	0.1
DJ08	0.6038	2.8637	0.1070	0.1
DJ09	0.4255	1.4218	0.0754	0.05
DJ10	0.4510	1.5972	0.0799	0.05
DJ11	0.5019	1.9786	0.0890	0.05
DJ12	0.6038	2.8637	0.1070	0.05
CJ06	0.5637	2.4957	0.0999	0.1
CJ07	0.6274	3.0916	0.1112	0.1
CJ08	0.7548	4.4746	0.1338	0.1
CJ09	0.53185	2.2216	0.0943	0.05
CJ10	0.5637	2.4957	0.0999	0.05
CJ11	0.6274	3.0916	0.1112	0.05
CJ12	0.7548	4.4746	0.1338	0.05

1. *Minimum dilution*

Cases DJ08 and CJ08 were selected to demonstrate the effect of R_{jc}, while four cases (DJ05 to DJ08) were chosen to show the impact of R_{aj}. Additionally, cases DJ02 and DJ10 were included as a comparison group to examine the effect of S_t relative to case DJ06. Before curve fitting for the cross-sectional minimum dilution (S_c), it was necessary to apply dimensionless processing to the relevant parameters and data to establish a relationship. For the exit distance parameter, x/L_m was used for dimensionless scaling. Similarly, for the cross-sectional minimum dilution, dimensionless processing was performed based on S_cd/L_m, resulting in FIG. 13. The length scale L_m can accurately represent the influence of R_{jc} and S_t on the minimum dilution [FIG. 13(a) and 13(c)]. However, the influence of R_{aj} cannot be characterized properly [FIG. 13(b)], indicating that the R_{aj} has a more pronounced effect and should be considered in the curve fitting.

Next, the w_0/w_{ch} is introduced to further emphasize the effect of R_{aj} [FIG.14]. The combination of L_m and w_{ch} can better characterize the variation of the cross-sectional minimum dilution (S_c). Consequently, the semi-empirical formula for the cross-sectional minimum dilution (S_c) of the oscillating jet in the current environment can be expressed as follows:

$$\frac{S_c d w_0}{L_m w_{ch}} = 1.55\left(\frac{x}{L_m}\right)^{0.5411} \qquad 0.2 < \frac{x}{L_m} < 5 \tag{17}$$

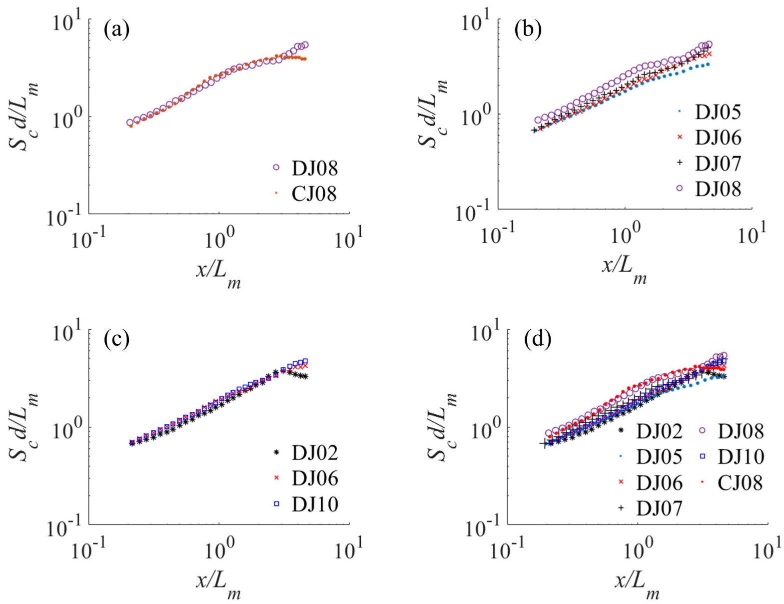

FIG. 13. Dimensionless relationship between minimum dilution S_cd/L_m and the downstream distance x/L_m, (a)-(c) the influence of R_{jc}, R_{aj} and S_t, (d) all cases.

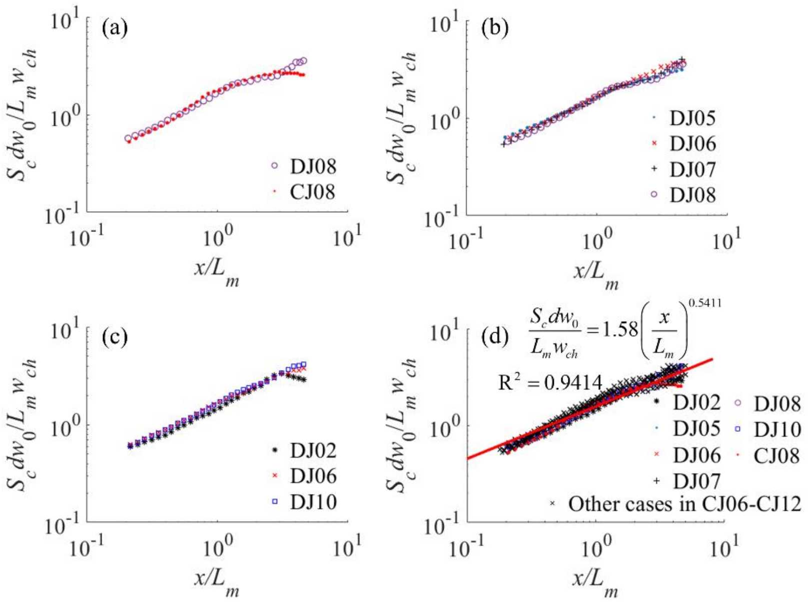

FIG. 14. Dimensionless relationship between minimum dilution $S_c dw_0/L_m w_{ch}$ and the downstream distance x/L_m, (a)-(c) the influence of R_{jc}, R_{aj} and S_t, (d) all cases.

2. Jet visible diffusion area

Similarly, the six cases are selected for the fitting analysis of the jet visual area ($A_{25\%}$) of the cross-section, and the related parameters and data were also made dimensionless as a basis to establish the relationship between them [FIG. 15]. For the exit distance parameter, x/L_m can be used for the dimensionless operation. For the exit distance parameter, x/L_m was used for the dimensionless scaling. Regarding the jet visual area, the dimensionless operation was performed based on $A_{25\%}/d^{0.2}L_m^{1.8}$. As shown in FIG. 15, the characteristic length L_m effectively characterizes the variation in the jet visual area. Consequently, the semi-empirical formula for the cross-sectional jet visual area ($A_{25\%}$) of an oscillating jet in a current environment can be expressed as follows:

$$\frac{A_{25\%}}{d^{0.2}L_m^{\ 1.8}} = 2.29\left(\frac{x}{L_m}\right)^{0.4941} \quad 0.2 < \frac{x}{L_m} < 5 \qquad (18)$$

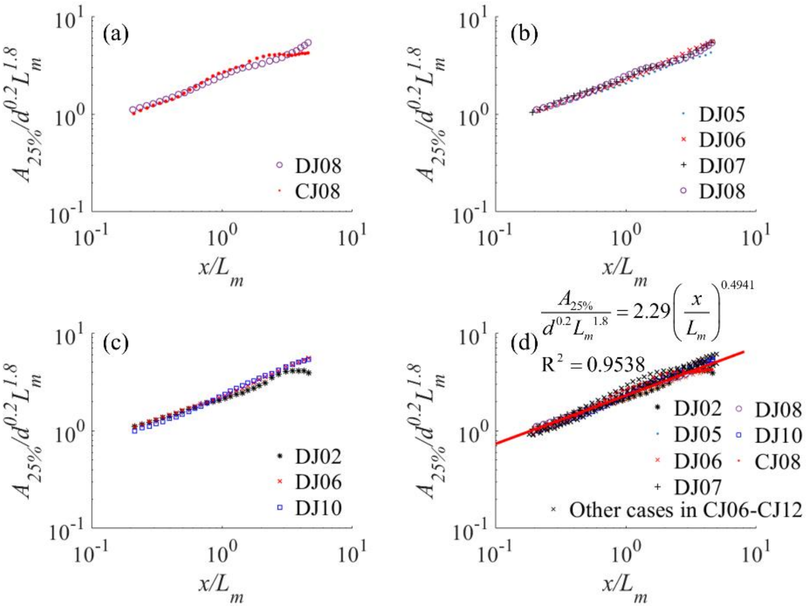

FIG. 15. Dimensionless relationship between jet visual area $A_{25\%}/d^{0.2}L_m^{1.8}$ and the downstream distance x/L_m, (a)-(c) the influence of R_{jc}, R_{aj} and S_t, (d) all cases.

E. Comparison of jet dilution law in different environments

The periodicity of waves is closely analogous to the oscillatory effects on the dilution characteristics of jets, allowing for a correspondence between the characteristic parameters of non-oscillating jets in wave-current coexisting environment and oscillating jets in the current environment. Specifically, the characteristic velocity of waves corresponds to the amplitude of oscillating jets, and the wave period matches the period of oscillations. The phenomenon of effluent clouds is a defining feature of non-oscillatory jets in wave-current coexisting environments, and the jet is divided into two distinct parts: an effluent cloud section and a jet bending section, distinguishing them from jets in current-only environment. Xu et al.[28] have elucidated the formation mechanisms and dynamics of pollutant clouds in non-oscillatory jets in wave-current coexisting environments. The wave oscillatory effect triggers the formation of effluent clouds, with their frequency corresponding to the wave frequency. In this study, similar conclusions were reached: the oscillatory effect of the jet in the current environment produces effluent clouds, and their frequency is consistent with that of the oscillating jet. These clouds exhibit the morphological characteristics of separation followed by merging.

In non-oscillatory jets in wave-current conditions and oscillatory jets in current environments, the dilution parameter increases with the increase of R_{jc} and R_{aj}, and with the decrease of S_t, indicating that oscillatory action effectively enhances the dilution capacity of the jet. In this study, we found the dilution parameter is most influenced by the mean velocity of the oscillating jet in the current environment. However, a higher mean velocity may cause the oscillating jet to prematurely impact the free surface of the downstream receiving water, reducing its dilution effect. Similar conclusions were drawn for non-oscillatory jets in wave-current coexisting environments. The key difference in dilution characteristics between the two environments is that oscillating jets diffuse more near the jet outlet and mix more intensively with the receiving water than in wave environments. Notably, the kinematic properties of non-oscillatory jets in wave-current coexisting environments are more affected by the S_t.[29] In contrast, for oscillating jets in current environments, mean jet velocity and amplitude are the primary parameters influencing kinematic properties, while the S_t has little effect on the dilution behavior of jets. This is due to the changes in amplitude and period directly impacting the morphology and motion of oscillating jets, reflecting the oscillatory effect in the water body. Conversely, in wave environments, the effects on the jet are indirect, with the influence of wave speed, period, and height radiating throughout the entire water body. This leads to differences in how each parameter affects the dilution behavior.

TABLE III provides empirical formulas for jet dilution in three different environments: a current-only environment, an oscillatory jet in a wave-current coexisting environment, and an oscillatory jet in a current environment. For cross-sectional minimum dilution (S_c), the formulas share a similar structure in the three environments, with $S_{c(0)}d/L_m$=$C_1(x/L_m)^{C2}$. However, for non-oscillatory jets in a wave-current coexisting environment and oscillatory jets in a current environment, the formulas account for wave periodicity (u_0/u_{ch}) and oscillatory effects (w_0/w_{ch}). The coefficient values for non-oscillatory jets in wave-current coexisting environments and oscillatory jets in current environments are very similar, indicating that the dilution laws are alike in both environments. In contrast, the fitting results for the cross-sectional jet visual area ($A_{25\%}$) show differences between non-oscillatory jets in wave-current coexisting environments and oscillatory jets in current environments. As previously analyzed, for oscillating jets in current environments, changes in S_t do not significantly affect the cross-sectional jet visual area. Consequently, S_t influences non-oscillating jets in wave-current coexisting environments but not in oscillating jets in current environments. Furthermore, in oscillating jets within current environments, the influence of R_{jc} is more prominent than that of R_{aj}. Therefore, only the characteristic length L_m is considered in the fitting of the formula for the cross-sectional jet visual area ($A_{25\%}$), simplifying the overall formula.

TABLE III. Summary of results of three concentration characteristic index formulas.

	Current-only environment[35]	Non-oscillating jets in the wave-current coexisting environment[29]	Oscillating jets in the current environment
Minimum dilution	$\frac{S_{c0}d}{L_m}=1.34\left(\frac{x}{L_m}\right)^{0.66}$ $0.2<\frac{x}{L_m}<6.5$	$\frac{S_c d u_0}{L_m u_{ch}}=0.9842\left(\frac{x}{L_m}\right)^{0.5773}$ $0.2<\frac{x}{L_m}<5$	$\frac{S_c d w_0}{L_m w_{ch}}=1.55\left(\frac{x}{L_m}\right)^{0.5411}$ $0.2<\frac{x}{L_m}<5$
Jet visual area	/	$\frac{A_{25\%}u_0^2 S_t^{0.5}}{d^{0.4}L_m^{1.6}u_{ch}^2}=0.8637\left(\frac{x}{L_m}\right)^{0.4405}$ $0.2<\frac{x}{L_m}<5$	$\frac{A_{25\%}}{d^{0.2}L_m^{1.8}}=2.29\left(\frac{x}{L_m}\right)^{0.4941}$ $0.2<\frac{x}{L_m}<5$

IV. CONCLUSIONS

In this study, the three-dimensional structures and mixing behaviors of a turbulent jet under various oscillating jet conditions in a current environment were investigated using large eddy simulation (LES). The main conclusions are as follows:

(1) Oscillating jets in current environments exhibit downstream displacement of the main flow line compared to non-oscillating jets, with higher impact heights of effluent clouds and more complete mixing between the jet and current.

(2) Increases in R_{jc} and R_{aj}, or a decrease in the S_t, lead to higher impact heights, larger minimum dilution and visual jet area for an oscillating jet in the current environment. Among these factors, the S_t has the least influence on jet dilution.

(3) Two semi-empirical equations for the initial dilution of oscillating jets in current environments were derived using dimensional analysis, incorporating characteristic velocity and length scales. The equations for cross-sectional minimum dilution (S_c) and the jet visual area ($A_{25\%}$) are presented as follows:

$$\frac{S_c d w_0}{L_m w_{ch}}=1.55\left(\frac{x}{L_m}\right)^{0.5411}\qquad 0.2<\frac{x}{L_m}<5$$

$$\frac{A_{25\%}}{d^{0.2}L_m^{\ 1.8}}=2.29\left(\frac{x}{L_m}\right)^{0.4941}\qquad 0.2<\frac{x}{L_m}<5$$

(4) The mixing characteristics of oscillating jets in current environments are similar to those of

non-oscillating jets in wave-current coexisting environments. The empirical formulas for initial dilution are structurally similar, suggesting that the oscillating jet's effects on the dilution pattern closely resemble those of wave-induced oscillation.

Overall, the results show that oscillating jets in current environments enhance pollutant dilution, making the oscillating jet mode a promising approach for the design of effluent diffusers, which provides a scientific reference for improving the initial dilution of industrial and domestic wastewater discharge.

ACKNOWLEDGMENTS

This work was partly supported by the National Natural Science Foundation of China (51979076).

AUTHOR DECLARATIONS

Competing Interests

The authors have no conflicts to disclose.

Author Contributions

W. Zhang provided LES modeling data, designed the study, analyzed and interpreted the results and drafted the manuscript; Z. Xu calculated and collected numerical experimental data, summarized the findings and revised the manuscript; S. Fang interpreted the results and revised the manuscript; S. Pan and Y. Chen revised the manuscript. All authors read and approved the final manuscript. The corresponding author had final responsibility for the decision to submit for publication.

DATA AVAILABILITY

The data that support the findings of this study are available from the corresponding author upon reasonable request.

REFERENCES

1. Y. Chen, Z. He, Y. Lou, H. Zhang, R. Zhu, and S. U. Okon, "Experimental study of horizontal heated buoyant jets in a linearly stratified ambience," Physics of Fluids 33, (2021).

2. A. K. Moawad, and N. Rajaratnam, "Dilution of circular turbulent nonbuoyant surface jets in cross-flows," Journal of Hydraulic Engineering 124, 474 (1998).

3. S. Muppidi, and K. Mahesh, "Study of trajectories of jets in crossflow using direct numerical simulations," Journal of Fluid Mechanics 530, 81 (2005).

4. S. Megerian, J. Davitian, L. d. B. Alves, and A. Karagozian, "Transverse-jet shear-layer instabilities. Part 1. Experimental studies," Journal of fluid Mechanics 593, 93 (2007).

5. D. Shao, and A. W. Law, "Mixing and boundary interactions of 30 and 45 inclined dense jets," Environmental fluid mechanics 10, 521 (2010).

6. M. Zeitoun, "Model Studies of Outfall Systems for Desalination Plants. Part III. Numerical Simulation and Design Considerations," (1972).

7. P. J. Roberts, and G. Toms, "Inclined dense jets in flowing current," Journal of Hydraulic Engineering 113, 323 (1987).

8. G. A. Kikkert, M. Davidson, and R. Nokes, "Inclined negatively buoyant discharges," Journal of Hydraulic engineering 133, 545 (2007).

9. P. J. Roberts, W. Snyder, and D. Baumgartner, "Ocean outfalls. I: Submerged wastefield formation," Journal of Hydraulic Engineering 115, 1 (1989).

10. P. J. Roberts, W. Snyder, and D. Baumgartner, "Ocean outfalls. III: Effect of diffuser design on submerged wastefield," Journal of Hydraulic Engineering 115, 49 (1989).

11. P. J. Roberts, and W. H. Snyder, "Hydraulic model study for Boston outfall. I: Riser configuration," Journal of Hydraulic Engineering 119, 970 (1993).

12. P. J. Roberts, and W. H. Snyder, "Hydraulic model study for Boston outfall. II: environmental performance," Journal of Hydraulic Engineering 119, 988 (1993).

13. A. C. Lai, D. Yu, and J. H. Lee, "Mixing of a rosette jet group in a crossflow," Journal of Hydraulic Engineering 137, 787 (2011).

14. J. J. Sharp, "THE USE OF A BUOYANT WALL JET TO IMPROVE THE DILLUTION OF A SUBMERGED OUTFALL," Proceedings of the Institution of Civil Engineers 59, 527 (1975).

15. G. C. Noutsopoulos, and P. C. Yannopoulos, "Axial Dilution in Obstructed Round Bouyant Jet," Journal of Hydraulic Engineering 115, 71 (1989).

16. M. Taherian, and A. Mohammadian, "Buoyant jets in cross-flows: review, developments, and applications," Journal of Marine Science and Engineering 9, 61 (2021).
17. C. Anghan, M. H. Bade, and J. Banerjee, "A review on fundamental properties of the jet in the wave environment," Ocean Engineering 250, 110914 (2022).
18. N. Mori, and K. A. Chang, "Experimental study of a horizontal jet in a wavy environment," Journal of engineering mechanics 129, 1149 (2003).
19. M. Mossa, "Experimental study on the interaction of non-buoyant jets and waves," Journal of Hydraulic Research 42, 13 (2004).
20. Y. Ryu, K. A. Chang, and N. Mori, "Dispersion of neutrally buoyant horizontal round jet in wave environment," Journal of Hydraulic Engineering 131, 1088 (2005).
21. L. Yuan, The three dimensional numerical simulation of vertical jet in waves (Springer, 2009).
22. K. A. Chang, Y. Ryu, and N. Mori, "Parameterization of neutrally buoyant horizontal round jet in wave environment," Journal of waterway, port, coastal, and ocean engineering 135, 100 (2009).
23. T. Webb, and R. B. Tomlinson, "Design procedures for effluent discharge to estuaries during ebb tide," Journal of environmental engineering 118, 338 (1992).
24. D. B. Sharp, A. Shawcross, and C. A. Greated, "LIF measurement of the diluting effect of surface waves on turbulent buoyant plumes," Journal of Flow Control, Measurement and Visualization 2, 77 (2014).
25. J. M. Chyan, and H. H. Hwung, "On the interaction of a turbulent jet with waves," Journal of Hydraulic Research 31, 791 (1993).
26. S. C. Hsiao, T. W. Hsu, J. F. Lin, and K. A. Chang, "Mean and turbulence properties of a neutrally buoyant round jet in a wave environment," Journal of waterway, port, coastal, and ocean engineering 137, 109 (2011).
27. Z. Xu, Y. Chen, J. Tao, Y. Pan, D. M. Sowa, and C. Li, "Three-dimensional flow structure of a non-buoyant jet in a wave-current coexisting environment," Ocean Engineering 116, 42 (2016).
28. Z. Xu, Y. Chen, Y. Wang, and C. Zhang, "Near-field dilution of a turbulent jet discharged into coastal waters: Effect of regular waves," Ocean Engineering 140, 29 (2017).
29. Z. Xu, Y. Chen, and Y. Pan, "Initial dilution equations for wastewater discharge: Example of non-buoyant jet in wave-following-current environment," Ocean Engineering 164, 139 (2018).

30. S. Fang, Y. Chen, W. Shi, Z. Xu, X. Zhou, and X. Xu, "Mixing behavior equations created by a buoyant jet in wavy crossflow environments," Physics of Fluids 36, (2024).

31. C. M. Hsu, and R. F. Huang, "Effects of acoustic excitation at resonance Strouhal numbers on characteristics of an elevated transverse jet," Experimental thermal and fluid science 35, 1370 (2011).

32. W. Marcum, S. Cadell, and C. Ward, "The effect of jet location and duty cycle on the fluid mechanics of an unconfined free jet and its heat transfer on an impinging plate," International Journal of Heat and Mass Transfer 88, 470 (2015).

33. A. Arote, M. Bade, and J. Banerjee, "On coherent structures of spatially oscillating planar liquid jet developing in a quiescent atmosphere," Physics of Fluids 32, (2020).

34. P. Lin, and C. W. Li, "A σ‐coordinate three‐dimensional numerical model for surface wave propagation," International Journal for Numerical Methods in Fluids 38, 1045 (2002).

35. H. Shi, G. Wang, X. Luo, J. Yang, and X. Y. Lu, "Large-eddy simulation of a pulsed jet into a supersonic crossflow," Computers & Fluids 140, 320 (2016).

36. J. Lu, and H. Dai, "Large eddy simulation of flow and mass exchange in an embayment with or without vegetation," Applied Mathematical Modelling 40, 7751 (2016).

37. X. Zhou, K. H. Luo, and J. J. Williams, "Large-eddy simulation of a turbulent forced plume," European Journal of Mechanics-B/Fluids 20, 233 (2001).

38. J. H. Lee, and V. Chu, Turbulent jets and plumes: a Lagrangian approach (Springer Science & Business Media, 2012).